Engineering Fracture Mechanics 197 (2018) 27–47

Contents lists available at ScienceDirect

Engineering Fracture Mechanics

journal homepage: www.elsevier.com/locate/engfracmech

On crack band model in finite element analysis of concrete fracture in engineering practice

J. Červenka[a,*], V. Červenka[a], S. Laserna[b]

[a] Červenka Consulting s.r.o., Prague, Czech Republic
[b] ETSIAM, Castilla-La Mancha University, Albacete, Spain

ABSTRACT

When finite element nonlinear analysis is applied to address the typical engineering problems such as ultimate load carrying capacity or serviceability limits such as deflections or crack width, a special care should be taken for the proper definition of the crack band namely in the presence of reinforcement.

The definition of crack band in tension should take into account the reinforcement spacing as well as finite element size. The crack band size should be also limited from below depending on the minimal possible spacing of micro-cracks. In compression failure an analogical concept to the crack band method can be introduced, but again the compressive band size should be limited from below depending on the characteristic dimensions of the analyzed structure.

The paper proposes three localization limiters for practical applications of nonlinear finite element model using the smeared crack approach and crack band method both for tension and compression.

The application of these localization limiters is demonstrated and verified on several problems ranging from shear failure, bending behavior and compressive failure. It is demonstrated that the simple application of these limiters can increase the accuracy of finite element analysis even if very small or very large finite element sizes are used, which is often necessity in practice or research and development.

1. Introduction

The pioneering work of Bažant and Oh [2] introduced the crack band approach to address the issue of proper energy dissipation in nonlinear finite element analysis of brittle materials such as for instance concrete. The method has become a standard approach in most commercial as well as scientific programs for advanced finite element modeling of concrete and reinforced concrete structures. Engineers often apply nonlinear analysis with crack band approach to solve practical engineering problems. This rapid development is also embraced by the development of new national and international design standards. For instance model fib [25] and Červenka [15] introduced for the first time a comprehensive system for the treatment of safety and model uncertainty for structural assessment and design based on nonlinear analysis.

Some concrete constitutive models also extend the crack band concept for the compression failure as experimentally discovered by Van Mier [33] and Nakamura and Higai [26], which is however questionable approach since the localization band in compression is a structural parameter rather than material parameter [7,10].

The crack band method is mostly applied within the framework of classical smeared crack approach, which was introduced

* Corresponding author.
E-mail address: jan.cervenka@cervenka.cz (J. Červenka).

https://doi.org/10.1016/j.engfracmech.2018.04.010
Received 12 March 2018; Accepted 6 April 2018
Available online 26 April 2018
0013-7944/

already in the 70's by landmark works of Ngo and Scordelis [27], Rashid [29] and Červenka and Gerstle [10]. Many material models for concrete and reinforced concrete were developed in 70's, 80's and 90's such as for instance the models by Suidan and Schnobrich [32], Lin and Scordelis [24], de Borst [17], Rots and Blaauwendraad [30], Pramono and Willam [28], Etse [21] or Lee and Fenves [23]. These models are based on the finite element method. A concrete material model is formulated as a special constitutive model that is used at each integration point for the evaluation of internal forces. It was soon realized that material models with strain softening, if not formulated properly, exhibit severe mesh dependency [18], and tend to zero energy dissipation if the element size is reduced [1].

The crack band approach was proposed by Bažant and Oh [2] to remedy the convergence towards zero energy dissipation. A more rigorous solution of the ill-posed nature of the strain softening problem is the introduction of nonlocal or higher-order continuum models: such as non-local damage model by Bažant and Pijaudier-Cabot [3], gradient plasticity model by de Borst and Mühlhaus [19] or gradient damage model by de Borst et al. [20]. The non-local models introduce additional material parameters related to an internal material length scale, which is however difficult to derive from existing material tests. Currently these models are mathematically rigorous, but are seldom used in engineering practice.

The limitations of the crack band model in practical engineering calculations, namely when it comes to large finite elements or in the presence of reinforcement, were clearly understood already in the work of Bažant and Oh [2]. However, the method limitations are seldom described, when it comes to using small finite elements. It is a critical limitation since in the finite element method, the model refinement is often used to prove the convergence of the numerical results to a unique solution. It can be argued that nonlocal approaches are addressing this issue by averaging or introducing an internal scale length, which represents a localization limiter.

The paper attempts to provide a comprehensive treatment of the problematic, when very large or very small finite elements are used in nonlinear simulations of reinforced concrete structure based on smeared crack models and crack band method.

2. Model for concrete

The main focus of this paper is on the modeling of tensile, shear as well as compressive damage localization and associated energy dissipation in reinforced concrete structures. The modeling of failure in reinforced concrete structures involves often complex failure mechanism including cracking, reinforcement yielding, bond failure between concrete and reinforcement as well as compressive crushing. Therefore at least a brief outline of the used material model is necessary. The used material model has been published in more details in Červenka et al. and Červenka & Papanikolaou [8,9].

The material model formulation is based on the decomposition of the strain vector into elastic $\bar{\varepsilon}_e$, plastic $\bar{\varepsilon}_p$ and fracturing $\bar{\varepsilon}_f$ strains, which for the incremental nonlinear solution can be written in the rate form as

$$\dot{\bar{\varepsilon}} = \dot{\bar{\varepsilon}}_e + \dot{\bar{\varepsilon}}_p + \dot{\bar{\varepsilon}}_f \tag{1}$$

The stress evolution is described by the formula:

$$\dot{\bar{\sigma}} = \mathbf{E}(\dot{\bar{\varepsilon}} - \dot{\bar{\varepsilon}}_p - \dot{\bar{\varepsilon}}_f) \tag{2}$$

In the above $\mathbf{E}$ is elastic stiffness and the two unknown strain vectors are defined as:

$$\dot{\bar{\varepsilon}}_f = \frac{\mathbf{E}}{\mathbf{E} + \mathbf{T}^{\mathrm{T}}\mathbf{E}_f\mathbf{T}}(\dot{\bar{\varepsilon}} - \dot{\bar{\varepsilon}}_p) \tag{3}$$

$$\dot{\bar{\varepsilon}}_p = \dot{\lambda}_p \bar{m}, \quad \dot{\lambda}_p = \frac{\bar{n}^{\mathrm{T}}\mathbf{E}(\dot{\bar{\varepsilon}} - \dot{\bar{\varepsilon}}_f)}{\bar{n}^{\mathrm{T}}\mathbf{E}\bar{m} - H_p},$$
$$\bar{n} = \frac{\partial F_p}{\partial \bar{\sigma}}, \quad \bar{m} = \frac{\partial G_p}{\partial \bar{\sigma}} \tag{4}$$

Eq. (3) represents the fracturing model, which takes into account the development of tensile cracks, while Eq. (4) corresponds to the plasticity model for the modeling of compressive concrete failure. These two equations are not independent and must be solved by an iterative algorithm, which is described in detail in [9].

2.1. Fracturing model

In the fracturing model, Eq. (3), the fracturing strain $\dot{\bar{\varepsilon}}_f$ is calculated from Eq. (2), where $\dot{\bar{\sigma}}$ is replaced by the stress in the cracks as defined in Eq. (5). $\mathbf{T}$ is the strain transformation matrix for transforming the strain vector from the global coordinate system into the local coordinate system aligned with cracks in concrete, and $\mathbf{E}_f$ is the stiffness matrix for the cracks. In the present model, maximum three orthogonal cracks can be modeled at each point, and the matrix $\mathbf{E}_f$ has the following form:

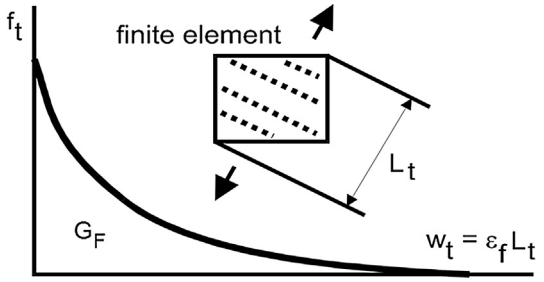

Fig. 1. Crack opening law of Hordijk 1991 and crack band L_t.

$$\dot{\bar{\sigma}}' = \mathbf{E}_f \dot{\bar{\varepsilon}}'_f,$$

$$\mathbf{E}_f = \begin{bmatrix} {}^{1}E_f & 0 & 0 & & & \\ 0 & {}^{2}E_f & 0 & & \mathbf{0} & \\ 0 & 0 & {}^{3}E_f & & & \\ & & & {}^{12}E_f & 0 & 0 \\ & \mathbf{0} & & 0 & {}^{23}E_f & 0 \\ & & & 0 & 0 & {}^{13}E_f \end{bmatrix} \tag{5}$$

where the prime symbols indicate the stress and strain quantities in the local coordinate system of the cracked concrete. The individual components of the matrix E_f are calculated by Eq. (6) using the softening evolution law (Fig. 1) for given value of the tensile strength f_t, which is a function of the crack opening displacement w_t. The crack band method of [2] is used, which allows to relate the crack opening displacement w_t to the fracturing strains $\bar{\varepsilon}_f$ through the crack band size L_t (Fig. 1). The shear components ${}^{ij}E_f$ of the matrix $\mathbf{E}_f$ are assumed to be dependent on the corresponding normal components and on the multiplier s_F, which is assumed to be an input material parameter.

$$\begin{aligned} {}^{i}E_f &= \frac{\partial f_t({}^{i}w_t)}{\partial w} L_t, \\ {}^{ij}E_f &= s_F \min({}^{i}E_f, {}^{j}E_f), \quad {}^{i}w_t = {}^{i}\varepsilon_f L_t \end{aligned} \tag{6}$$

The transformation matrix $\mathbf{T}$ is gradually calculated at the onset of cracking in each of the three material directions. This corresponds to the fixed crack model, when the crack direction is fixed after the initiation. On the other hand, if the matrix $\mathbf{T}$ is recalculated for each step based on direction of the current principal strains, a rotated crack model is recovered. It should be also noted that the evaluation of the fracturing model, i.e. Eqs. (3) and (6) requires an iterative algorithm since $\mathbf{E}_f$ depends $\bar{\varepsilon}_f$. This algorithm is described in detail in [9].

2.2. Plasticity model

In the plasticity model, Eq. (4), the plastic strain rate $\dot{\bar{\varepsilon}}_p$ is calculated from the consistency condition. λ_p is the plastic multiplier, and $\bar{n}$ and $\bar{m}$ are stress derivatives of the plastic and potential surface respectively. The plastic surface F_p is defined by the three-parameter criterion, (f_c, f_t, e), according to Menetrey & Willam [34] (Fig. 2).

$$F_p = \left[\sqrt{1.5} \frac{\rho}{\frac{\rho}{\widehat{f_c}}} \right]^2 + m \left[\frac{\rho}{\sqrt{6}\widehat{f_c}} r(\theta, e) + \frac{\xi}{\sqrt{3}\widehat{f_c}} \right] - c = 0 \tag{7}$$

$$m = 3 \frac{\widehat{f_c} - f_t^2}{\widehat{f_c} f_t} \frac{e}{e+1}$$

$$r(\theta, e) = \frac{4(1-e^2)\cos^2\theta + (2e-1)^2}{2(1-e^2)\cos\theta + (2e-1)[4(1-e^2)\cos^2\theta + 5e^2 - 4e]^{\frac{1}{2}}}$$

In the above equations, (ξ, ρ, θ) are the Haigh-Westergaard stress coordinates and f_c and f_t are the compressive strength and tensile strength, respectively. Parameter $e \in (0.5, 1.0)$ defines the roundness of the Menétrey-Willam failure surface, with a recommended value $e = 0.52$. The plastic surface is not constant. Its evolution is governed by the equivalent plastic strain ε_{eqp} (Fig. 3):

$$\dot{\varepsilon}_{eqp} = \min(\dot{\varepsilon}_{p1}, \dot{\varepsilon}_{p2}, \dot{\varepsilon}_{p3}) \tag{8}$$

where ε_{pi} is the i-th component of the principal plastic strains. The hardening is modeled by adjusting the compressive strength $\widehat{f}$, while the softening is controlled through the parameter c:

hardening $\epsilon_{eqp} \in < -\epsilon_{cp}\ ; 0 >$

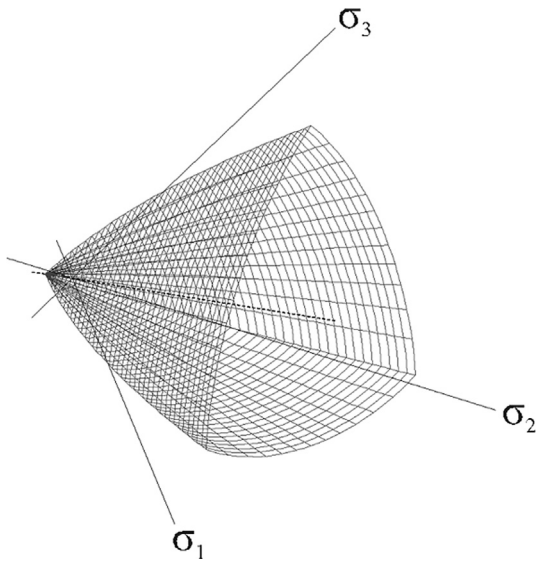

Fig. 2. Visualization of the three-parameter Menetrey & Willam [34] three-parameter concrete failure criterion.

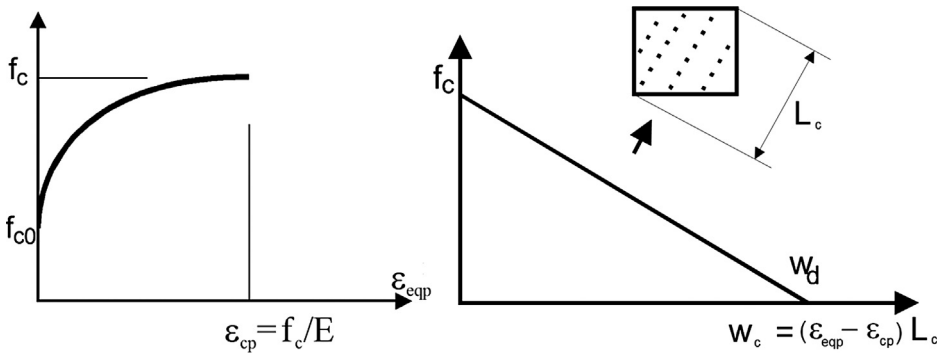

Fig. 3. Hardening law and softening law for the plasticity model for concrete in compression.

$$\widehat{f}_c(\varepsilon_{eqp}) = f_{c0} + (f_c - f_{c0})\sqrt{1-\left(\frac{\varepsilon_{cp}-\varepsilon_{eqp}}{\varepsilon_{cp}}\right)^2} \tag{9}$$

softening $\varepsilon_{eqp} \in \langle -\infty; -\varepsilon_{cp} \rangle$

$$\begin{aligned} &c = \left(1-\frac{w_c}{w_d}\right)^2, \quad w_c \in \langle -w_d; 0 \rangle \\ &c = 0, \quad w_c \in (-\infty; w_d) \\ &w_c = (\varepsilon_{eqp}-\varepsilon_{cp}) L_c \end{aligned} \tag{10}$$

In the above formulas, ε_{cp} is the value of the plastic strain, when the compression strength f_c is reached in a uni-axial compression test. f_{c0} is the onset of nonlinear behavior in compression, w_d is the critical value of compressive displacement and w_c is the crushing displacement analogical to crack opening displacement, but with different sign. When concrete crushing enters into the softening regime, an analogous approach to the crack band model is also used for the localization in compression within the crushing band L_c.

The plastic potential (11) defines the direction of the plastic flow, and is controlled by the parameter β, which defines the volumetric change during the crushing process: $\beta > 0$ means volume expansion, $\beta < 0$ material compaction, $\beta = 1$ material volume is preserved

$$G_p(\overline{\sigma}) = \beta\frac{1}{\sqrt{3}}I_1 + \sqrt{2J_2} \tag{11}$$

I_1 is the 1st invariant of stress vector and J_2 is the 2nd invariant of deviatoric stress vector. The hardening/softening modulus H_p from (4) is defined as

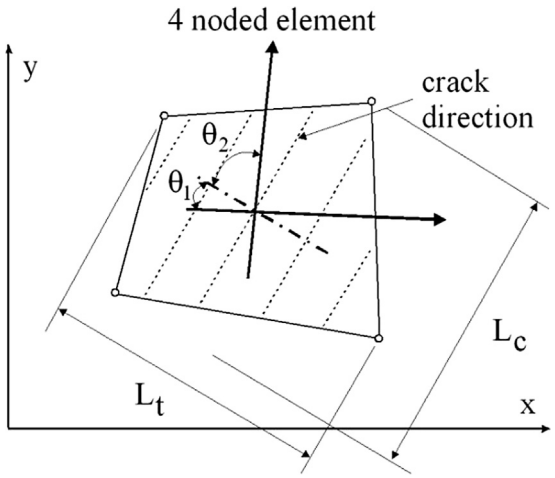

Fig. 4. Crack and crush band definition.

$$H_p = \frac{\partial F_p}{\partial f_c}\frac{\partial f_c}{\partial \varepsilon_{eqp}}\frac{\partial \varepsilon_{eqp}}{\partial \lambda_p} + \frac{\partial F_p}{\partial c}\frac{\partial c}{\partial w_c}\frac{\partial w_c}{\partial \lambda_p} \tag{12}$$

The briefly presented material model is described in more detail in Červenka and Papanikolaou [9], where the model was validated on various problems ranging from tension and compression tests up to shear or bending failures in reinforced concrete structural elements. The model is implemented in software ATENA [12]. The model has been validated by numerous benchmark competitions, the most recent one organized by Prof. Collins from Toronto University. The model provided the best prediction among 66 participants of the shear strength of a 19 m span and 4 m high reinforced concrete beam [6].

3. Crack band model for tensile and compressive softening

In the presented model, the softening in tension is controlled by the exponential law (Fig. 1) and the softening in compression is controlled by the linear law as shown in Fig. 3 and Eq. (10), in which the parameter c of the criterion (7) is reduced as a function of the crushing displacement w_c, which has an analogous meaning to the crack opening w_t (Fig. 1).

The tensile band L_t is calculated for each finite element as the element length projected into the normal crack direction. This is with agreement with the crack band model as proposed by Bažant and Oh [2]. An analogical approach can be used also for the compressive softening as schematically depicted in Fig. 4. This modeling approach to compression softening has been introduced by [8]. The crushing band L_c is calculated for each finite element as the element size projected into the direction of the minimal compressive stress. This model is based on the work of Van Mier [33] and Nakamura and Higai [26], where it was experimentally shown that a unique value of the post-peak critical crushing displacement w_d was recovered for the tested specimens independent of their sizes.

In order to address situations, when the crack direction is not perfectly align with the finite element edges as shown in Fig. 5, it was proposed by Červenka et al. [14] to modify the crack band direction depending on the orientation of the crack with respect to the finite element edges using the factor γ as described in Eq. (13). With this approach it is possible to partially eliminate the mesh orientation bias of the smeared crack modeling approach. When cracks propagate in a diagonal manner with respect to the mesh, the crack band is increased, which effectively means the material response becomes more brittle and it triggers the localization of diagonal cracks. This model is sufficient and was verified to provide reasonable accurate results for low order elements [14]. For other element types such as higher order elements more refined approach was proposed by [31]. In the presented study only low order finite elements with standard gauss quadrature will be used so these more refined methods will not be presented here.

$$\overline{L}_i = \gamma(\theta) L_i, \quad \theta = \min\{\theta_i\} \tag{13}$$

where

$$\gamma(\theta) = \gamma_{\max}\frac{\theta}{\theta_{\lim}}, \quad \theta \in \langle 0;\theta_{\lim}\rangle, \quad \theta_{\lim} = \pi/4, \quad \gamma_{\max} = 1.5 \tag{14}$$

4. Crack band limiters

In its basic form the crack band method assumes that a single localization band or crack appears inside each finite element when the crack fully develops. This is schematically shown in Fig. 6. The constitutive formulation of each element is modified in such a way that the correct crack opening law is recovered when the element undergoes the fracturing process. This was the brilliant idea of the

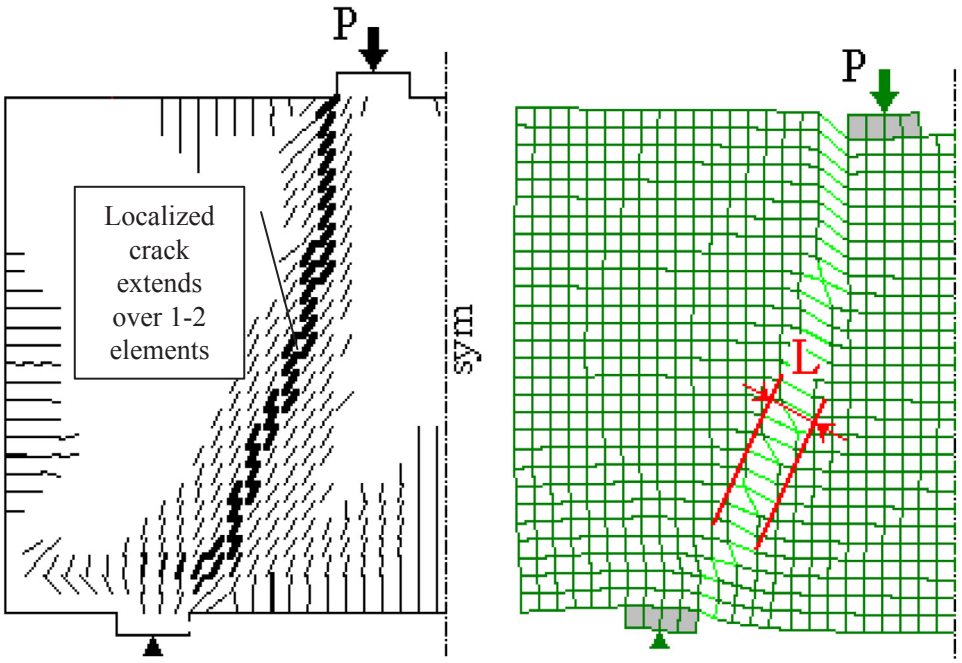

Fig. 5. Physical reasoning behind the crack band extension for cracks not parallel with the finite element edges.

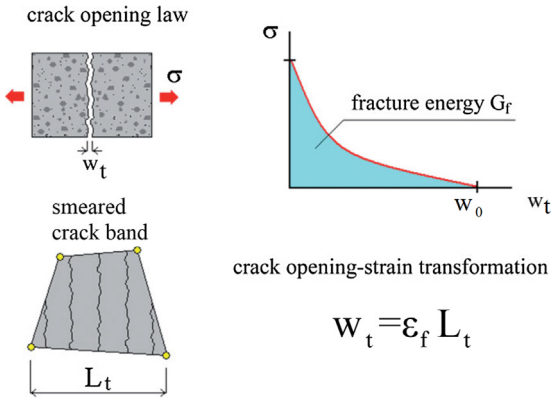

Fig. 6. Single crack assumption in the basic form of the crack band model.

original crack band model [2]. In the original paper this was accomplished mainly by the adjustment of the softening modulus. Alternatively this is facilitated by the transformation between crack opening displacement and strains using Eq. (6) for tension and Eq. (10) for compression.

It was already recognized by Bažant and Oh [2] that problems may occur when the finite element is too large or the fracture energy G_F is too low such that a snap back may occur on the constitutive level. It was proposed to reduce the tensile strength such that the snap back does not occur. In most practical engineering applications of the crack band approach, it is applied for the analysis of reinforced concrete structures, where two additional limits may appear:

(1) finite element size is larger than the maximum crack spacing,
(2) finite element size is smaller than the minimum crack spacing possible.

The first limit is typically the consequence of reinforcement diameter, cover and spacing. This situation is described in Fig. 7, which shows that if the depicted shear panel would be analyzed with finite element sizes smaller than 100 mm, the assumption of the crack band remain valid, i.e. maximum one crack can localize inside a finite element. On the contrary, if larger finite element sizes are used, such as for instance 300 mm, the assumption of the single crack is not valid, since due to the reinforcement arrangement the final maximum crack spacing is much smaller than the used element and three cracks will localize inside the finite element. In practice, this can easily happen as shown for instance in Fig. 8, where due to practical reasons it is more efficient to use relatively

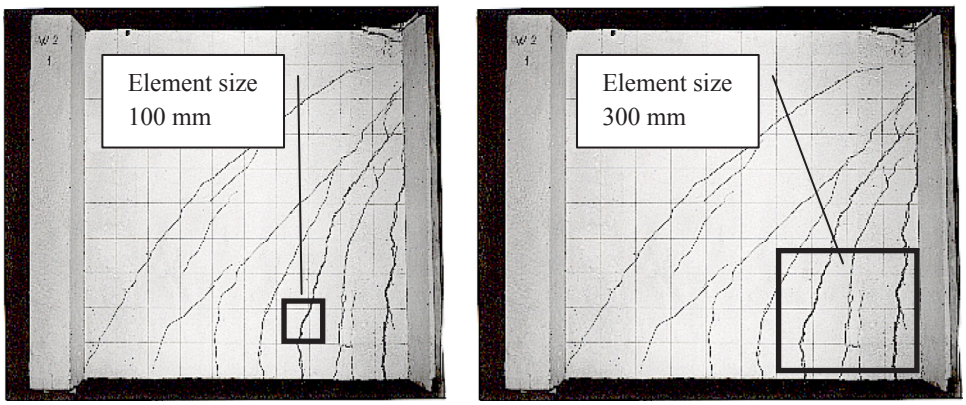

Fig. 7. Crack band size and crack spacing, when large finite element sizes are used, the assumption of single crack localization inside a finite element is not valid.

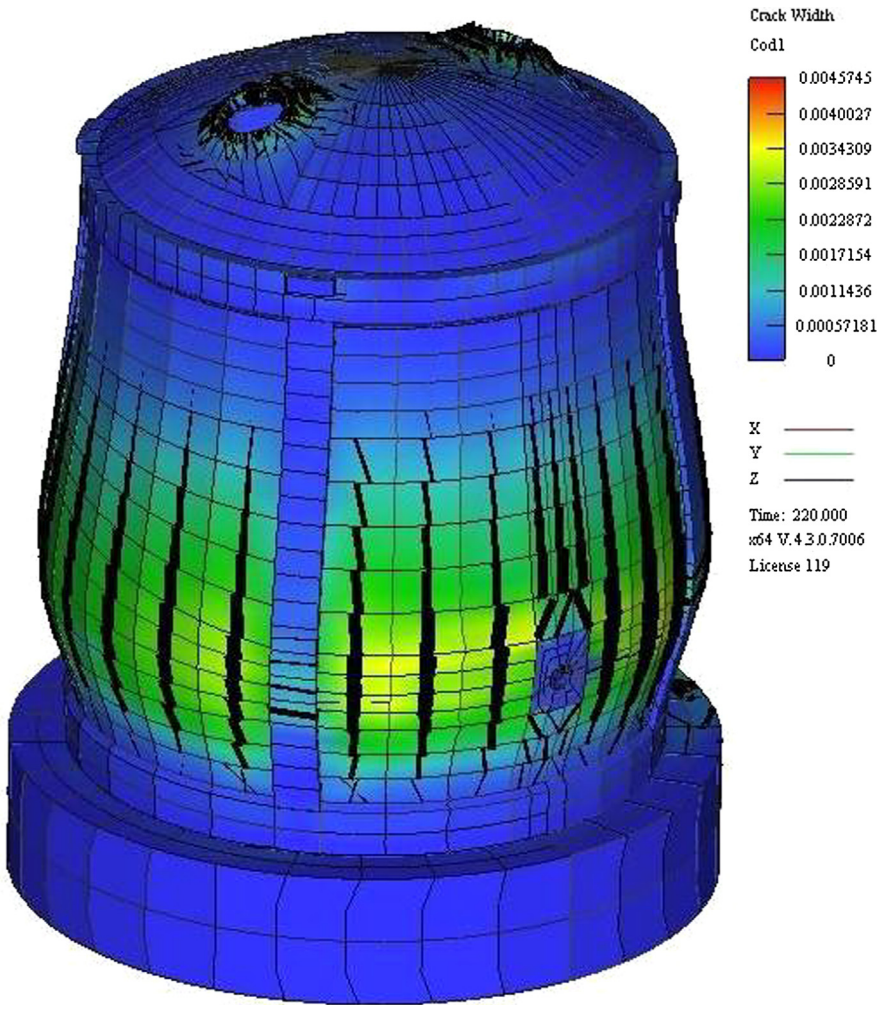

Fig. 8. Smeared crack modeling of a nuclear containment wall with element sizes larger than 3 m, where due to reinforcement, the assumption of single crack localization in one element cannot be valid.

large quadratic finite elements that can be much larger than the optimal size of 100 mm.

The second limit appears, when very small finite elements are used. This situation is schematically depicted in Fig. 9. It shows a hypothetical case, yet very typical in reinforced concrete structures, when tensile cracks are initiated around steel reinforcement.

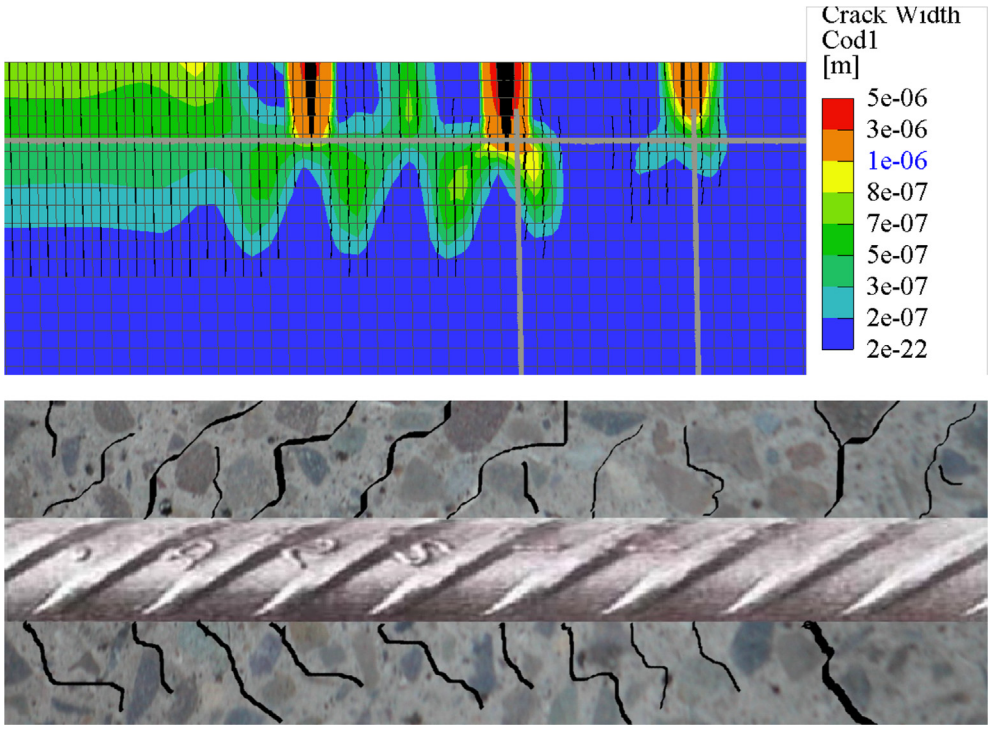

Fig. 9. Crack initialization with incorrect spacing when very fine mesh is used, top – crack initialization with extremely fine spacing due to very small element size, bottom – due to aggregate size or reinforcement rib spacing cracks can initialize only at certain minimal distance.

Very fine set of micro-cracks is first initiated, which later and further away from the rebar coalesce and form a macro-crack. The spacing of these initial micro-cracks is however limited by the aggregate sizes and/or distance of the bar ribs. In typical reinforced concrete structure such a limit is 20–30 mm. In a hypothetical numerical model, which is shown at the top of Fig. 9, it may happen that an extremely fine mesh is used. In this case, it is about 5 mm, which results in the initiation of much more micro-cracks than physically possible. This means that more energy is dissipated in these initial stages before the macro-crack fully develops. The consequence is that stiffer response is obtained. Smaller deflections are be calculated and the calculated crack widths are be underestimated.

It may be argued that the probability of using such small elements is very low and will not occur in practical cases. This may be true for the modeling of large scale structures, but for modeling structural details or when simulating laboratory experiments this can happen quite easily. The smallest dimension in laboratory experiments is often in the order of 100–300 mm. In such cases, finite meshes with element sizes of the order of 5–10 mm may be easily created. The computers are becoming powerful and the analysts often create very fine models hoping to obtain better results, while the outcome is quite opposite.

The both limitations on the crack band approach apply also to the case of compressive softening. In compression, however, the second limit is more critical. Extremely large finite elements would have to be used to reach a case, when more compression softening zones would localize inside a finite element. On the contrary, the opposite situation may occur very frequently. The crush band approach proposed by Červenka et al. [8] and Červenka et al. [7,10] captures the concrete response in compression if the size of the finite element is significantly larger than the size of the zone of the expected compressive localization. This is documented in Figs. 10 and 11. Fig. 11a shows the response of [26] experiments of compression cylinders with the same cross-sectional area but with different lengths (Fig. 10). The numerical results in Fig. 11a were calculated by models with only a single finite element. This is identical to assuming a macroscopic model with only single material point. As can be seen in Fig. 11a, the results correspond very well with the experimental evidence, and the size effect is correctly reproduced, i.e. the larger specimens exhibit more brittle behavior (see Fig. 12).

If the same cylindrical tests are, however, modeled with smaller elements (Fig. 10) using identical material parameters totally incorrect response is recovered (see Fig. 11b). In order to recover the correct responses as shown in Fig. 11a, it is necessary to use a value of $L_c = 150$ mm in Eq. (10). Interestingly this value corresponds to the diameter of the cylinders, and is also in agreement with the length of the damaged zones reported in [26], where it approximately corresponds to the diameter of the investigated cylinders.

Based on the above discussions it is proposed to introduce the following limits on the band size in tension and compression:

$$L_{t,\min} \leqslant \overline{L}_t \leqslant L_{t,\max} \tag{15}$$

$$L_{c,\min} \leqslant \overline{L}_c \tag{16}$$

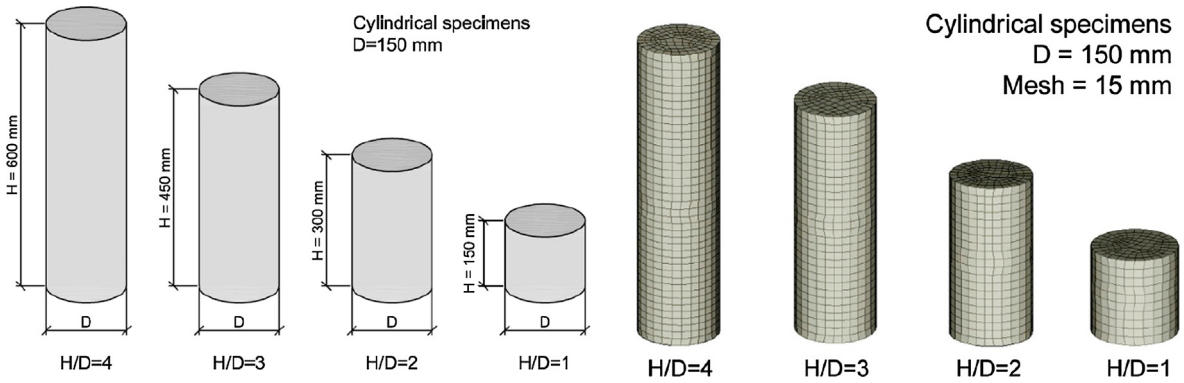

Fig. 10. Cylindrical specimens for [26] tests. (left) geometry, (right) mesh.

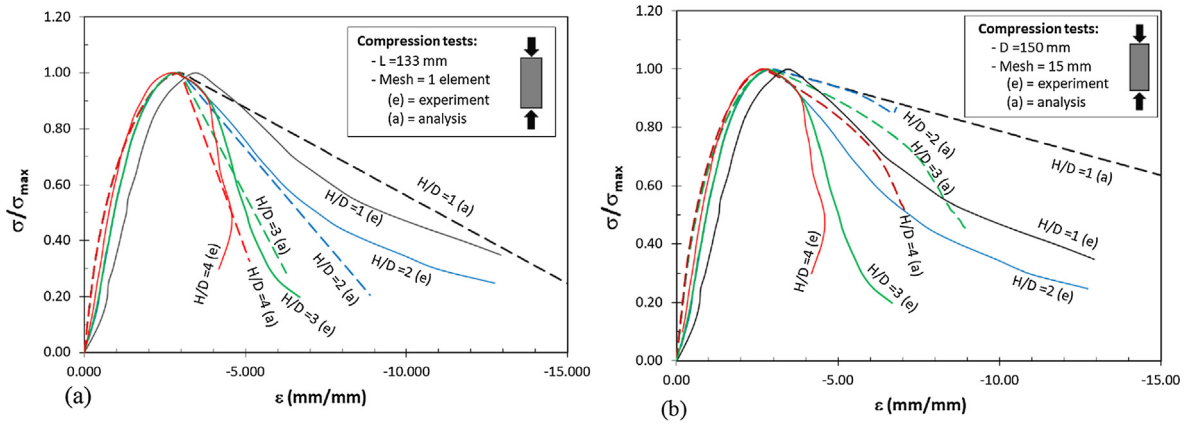

Fig. 11. Comparison of experimental and numerical results for direct compression tests of [26] for different specimen lengths, (a) single element model, (b) mesh size 15 mm.

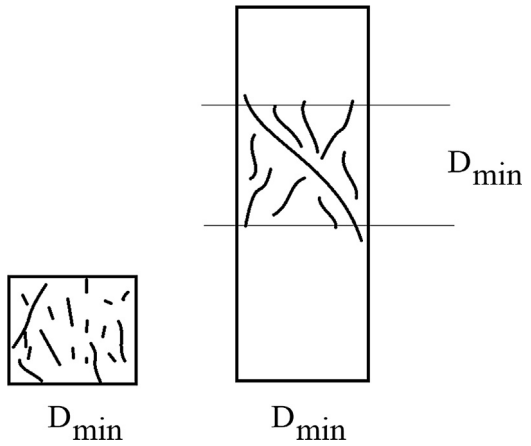

Fig. 12. Crush band relation to the minimal size of the compression zone in typical uni-axial compression tests with different specimen length.

If the calculated band size is outside of these limits the corresponding localization limiter should be used.

The localization limiters for tension can be relatively well estimated following the previous discussions. The minimal limiter in tension should be related to the internal structure of the material and can be recommended as 1.5 a_g, where a_g is the aggregate size.

The maximal limiter for tension should correspond to the typical crack spacing s_c. It can be estimated from spacing of reinforcement in each structural element.

The minimal localization limiter for compression cannot be directly related to the material structure. This parameter was investigated by Červenka et al. [7,10]. The limiter should be related to the dimensions of the compression zone and internal friction

Table 1
Recommended values for the localization limiters.

Localization limiter	Recommended value	Typical range	Note
Tension			
$L_{t,\min}$	1.5 a_g	10–50 mm	This is in good agreement with the recommendations used in nonlocal or gradient enhanced concrete models [3,19]
$L_{t,\max}$	s_c	150–300 mm	This value can be approximately estimated as the spacing of reinforcement in the walls/slabs or stirrups distance in beams or columns. More accurately it can be estimated using the standard code formulas for crack spacing, i.e. for instance from fib [25]
Compression			
$L_{c,\min}$	$D_{\min}$	150–1000 mm	Smallest dimension of the structural element in the section of interest

angle. The final size of the compression zone is difficult to know beforehand so the conservative assumption would be to use the minimal dimension of the investigated structural element.

The proposed limiters are summarized in Table 1. Considering the fact that the accurate definition of the localization limiters is very difficult and rather empirical, it could be argued that the best solution would be to use finite element sizes such that they are safely inside these limits. By close examination of the typical values for these parameters in Table 1, it is possible to see that this would be only the case of mesh size around 150 mm. It is interesting to note that this ideal size corresponds well to the dimensions of the standardized tests for the determination of the basic macroscopic concrete parameters such as: cubic compressive strength, tensile strength or fracture energy.

It is quite clear that such limitations on finite element size would be totally impractical, i.e. too small for the analysis of real life structures. On the contrary, for the simulation of laboratory experiments such finite element size would be often too large.

The proposed definition of the localization limiters in tension and compression to be used within the framework of smeared crack approaches and finite element method is documented on several examples in the following Section 6.

5. Validation and demonstration of the localization limiters

The behavior of the presented crack band and crush band definition as well as the importance of suitable localization limiters will be documented on several examples.

5.1. Reinforced concrete shear panel

The first example is the reinforced concrete shear panel in Fig. 13 tested by Červenka and Gerstle [11]. This example is modeled with different element sizes to show that the accuracy of results will start to deteriorate when too small or too large elements are used.

The used meshes are shown in Fig. 14. It should be noted that the model includes only the symmetrical half of the experiment. Linear quadrilateral elements are used. Fig. 13 shows the quadrilateral mesh with thin lines and the reinforcement modeled as embedded truss elements by solid lines. The material parameters as well as the used localization limiters are listed in Table 2 for all examples presented in this paper. The load-displacement curves are shown in Fig. 15 for the analyses without the limiters and in Fig. 16 for the case with the limiters. It is easy to observe that for mesh size 30 mm, which is exactly equal to the used tensile limiter

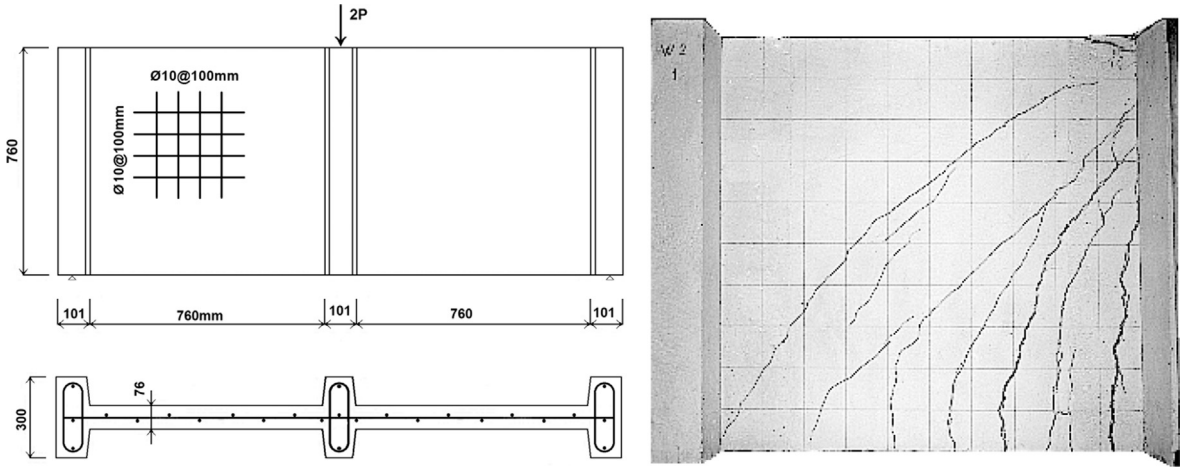

Fig. 13. Shear panel experiment and the obtained crack pattern on the symmetrical half.

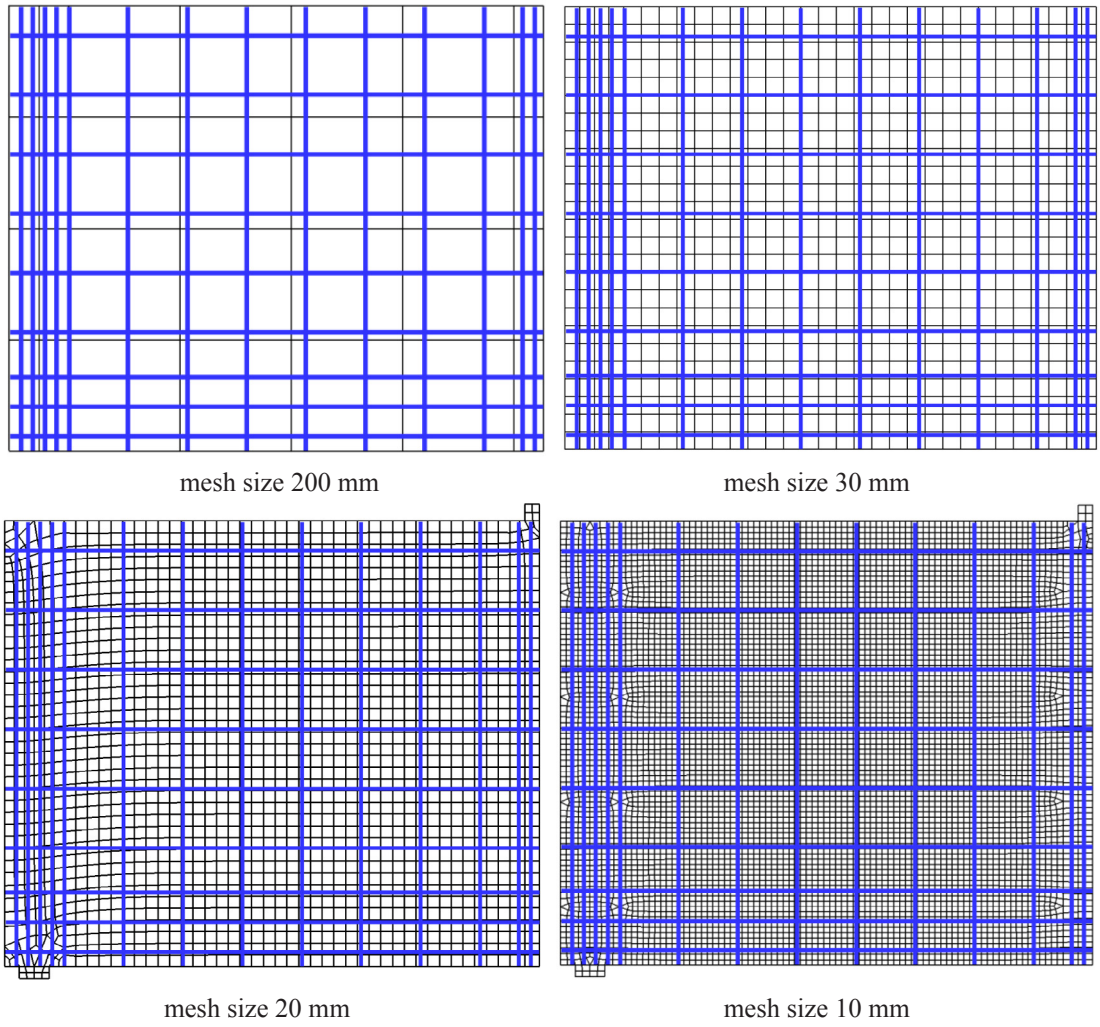

Fig. 14. Finite element meshes used for the shear panel example.

Table 2
Material parameters used in the examples.

Parameter	Comp. tests on cylinders	Shear panel	Crack width experiments	Flexural tests on beams
E (MPa)	20,000	20,250	30,000	22,000
μ	0.2	0.2	0.2	0.2
f_c (MPa)	20.0	28.5	27	27.8
f_t (MPa)	1.6	3.1	2.14	2.2
ε_{cp} (mm/mm)	0.002	0.0013	0.0014	0.000933
G_F (N/m)	125.0	58.0	50	55.0
β	0.5	0.5	0.5	0.5
w_d (mm)	2.5	2.5	2.5	2.5
Localization limiters				
$L_{t,min}$ [mm]	N/A	30	30	30
$L_{t,max}$ [mm]	N/A	150	150	30
$L_{c,min}$ [mm]	150	150	150	H/2*
Reinforcement				
σ_y [MPa]	N/A	353	550	565
σ_t [MPa]	N/A	420	578	590

* The compressive localization limiter determined as minimal element dimension from.

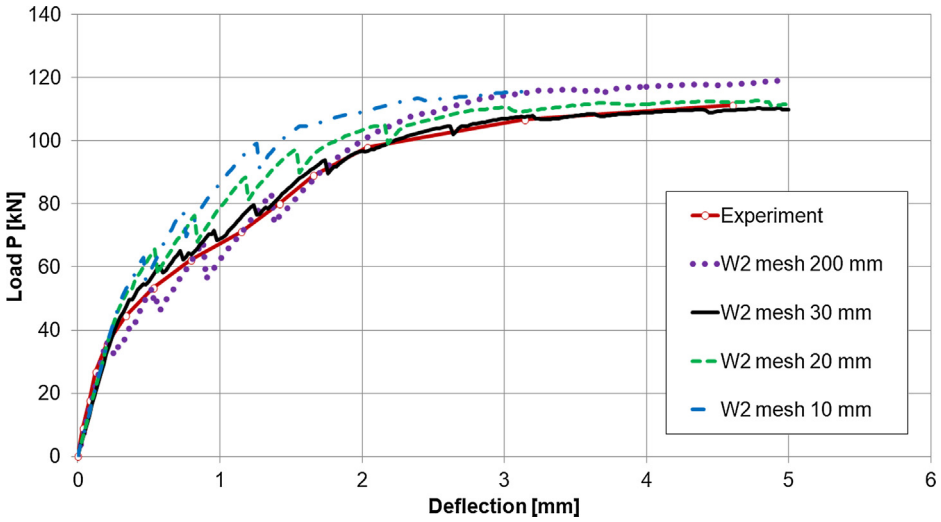

Fig. 15. Load-displacement diagrams for the shear panel example for different mesh sizes without crack spacing limiters.

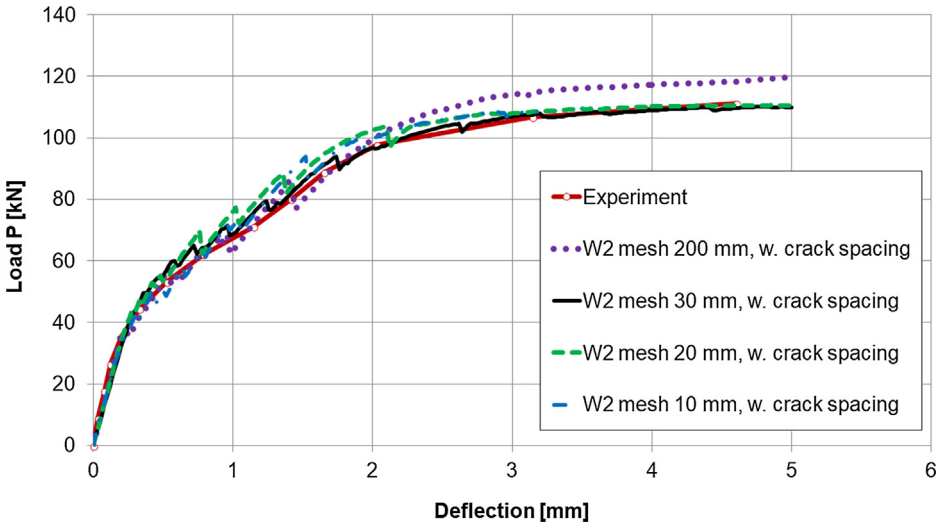

Fig. 16. Load-displacement diagrams for the shear panel example for different mesh sizes with crack spacing limiters.

0.03 (Table 2), the best agreement is obtained. For the largest size of 200 mm, it is possible to see that the results start to deteriorate. After the cracking initiation, i.e. in the range 0.2–1 mm the response is more brittle then experiment. This is because this element size is larger than $L_{t,\max}$ (150 mm) so more than one crack should be localizing at the bottom elements. Also stiffer response is obtained on the yield plateau, which can be attributed to the fact that this extremely coarse mesh does not have sufficient integration points at the top right hand corner to properly capture the compression zone. When smaller mesh size is used it is possible to see that the results on the yield plateau improve, but in the crack initiation stage, i.e. deflection 0.2–1 mm significantly stiffer response is obtained. This is quite clear for the finest mesh (size 10 mm). This mesh is about 3 times smaller than the tensile limiter and shows significant increase in stiffness in the hardening stage of the load-displacement diagram. This means that if no localization limiters would be use, the ideal mesh size for this analyses would be 30–150 mm.

Fig. 16 shows the load-displacements for the case when localization limiters are used. In this case it is possible to see that the results become almost identical for all meshes, with the exception that the coarsest mesh is not able to fully reproduce the peak load.

Fig. 17 shows the crack pattern and calculated crack widths at the last step in the analysis, which corresponds to the deflection of 5 mm. Fig. 17 compares the crack patterns for different meshes without and with the proposed localization limiters. The figure clearly shows that only results when crack spacing limiters are used shows similar crack patterns and crack widths for different mesh sizes that correspond well to the experimental observation (see Fig. 13). The results also show that the cracking starts as a shear dominated behavior. The final failure is however dominated by crushing of concrete at the top of the diagonal shear strut. This is documented in Fig. 18 by plots of equivalent plastic strain, which is defined in Eq. (8).

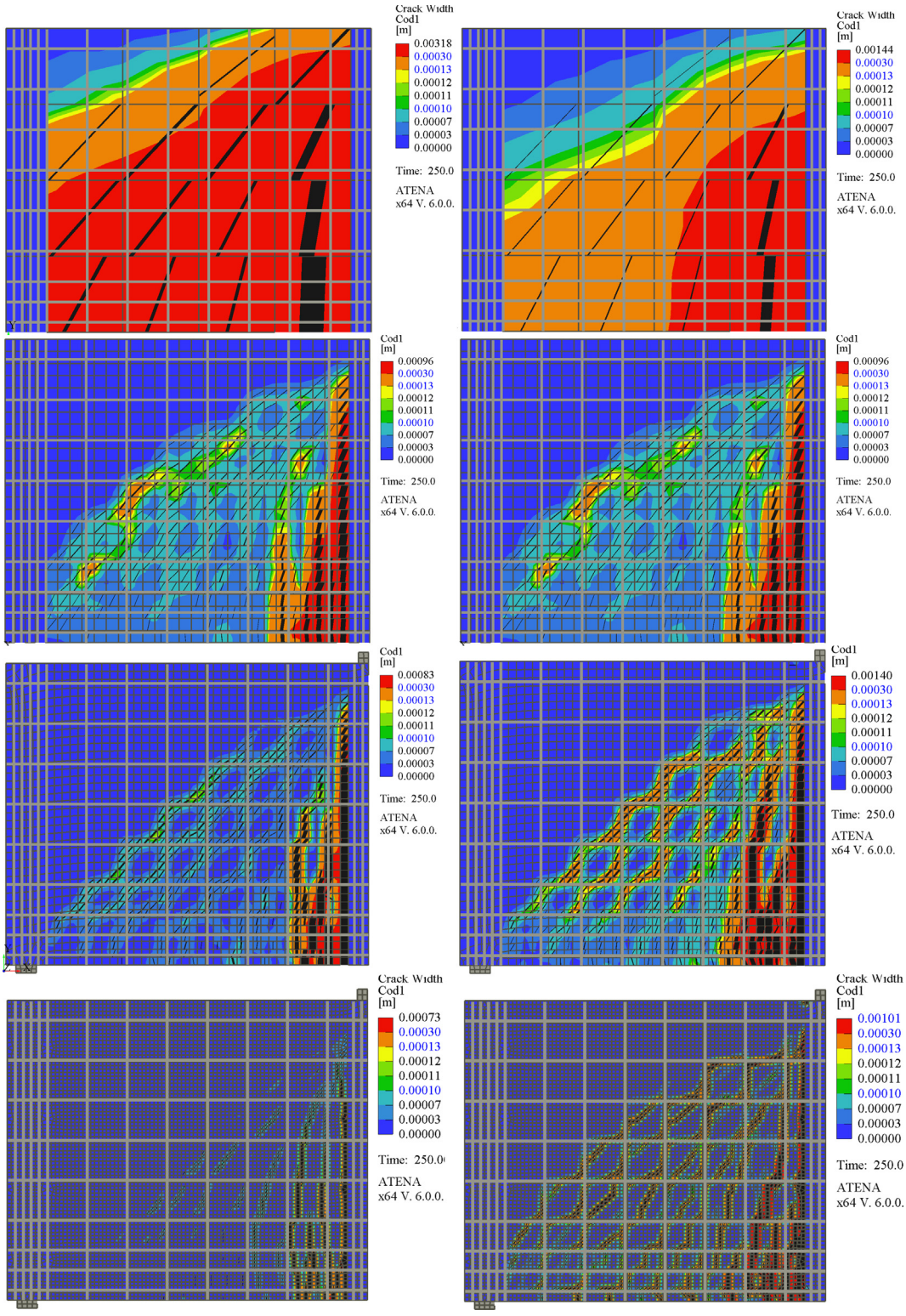

Fig. 17. Crack pattern and crack width for shear panels for different meshes (200, 30, 20, 10 mm) without (left) and with (right) crack band limits.

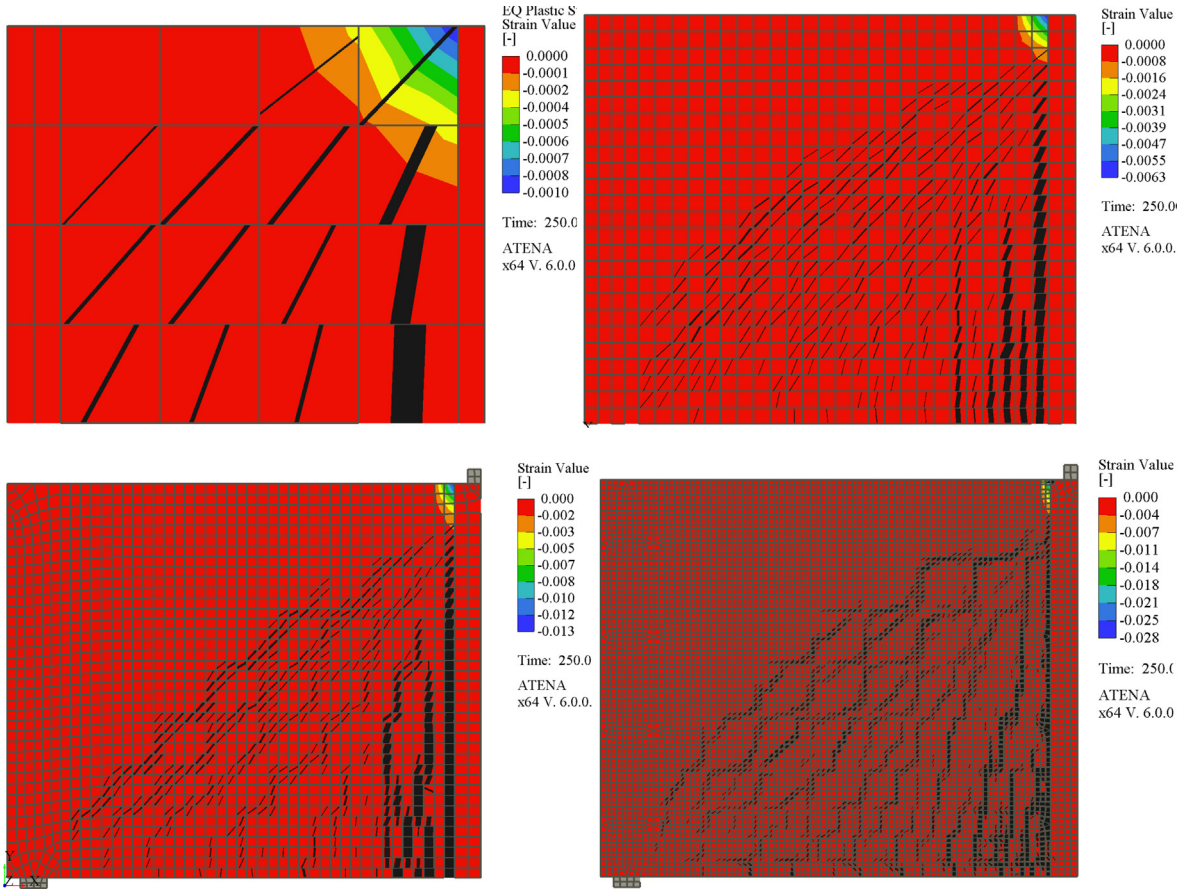

Fig. 18. Compressive crushing for shear panels for different meshes and without crack band limits.

5.2. Crack width bending experiment

The second example corresponds to one specimen from the test series of Caldentey et al. [5]. The four point bend beams have a cross section dimension (0.35 × 0.45 m) and span of 3.42 m (see Fig. 19). In the original test series the influence of variable reinforcement and cover was studied in order to determine its effect on crack spacing and crack width. The whole series was analyzed and numerically investigated by Červenka et al. [13,16] in order to evaluate the predictive capability of numerical simulation for the determination of crack spacing and crack width. In this paper, one of the beams with the reinforcement diameter 12 mm and concrete cover 70 mm is selected to demonstrate the effect of the localization limiters. Due to the size of the beam it is possible to test mainly the minimal localization limiter. The material parameters are again listed in Table 2. The tensile and softening minimal localization limiter was set to 30 mm and 150 mm respectively. The maximal crack spacing for this case is approximately 150 mm. In order to test this limit only two elements would be required along the beam height, which would not be sufficient for any meaningful finite element analysis. The finite element meshes used in this study are shown in Fig. 20. The obtained load-displacement curves are shown in Figs. 21 and 22 for the case without the spacing limiters and with the limiters respectively. The results document the similar behavior as it was observed already in the shear panel example. The crack spacing limiters do not influence significantly the final strength of the beams, but significant difference is observed in the stiffness of the response when the cracking is initiated, i.e. for

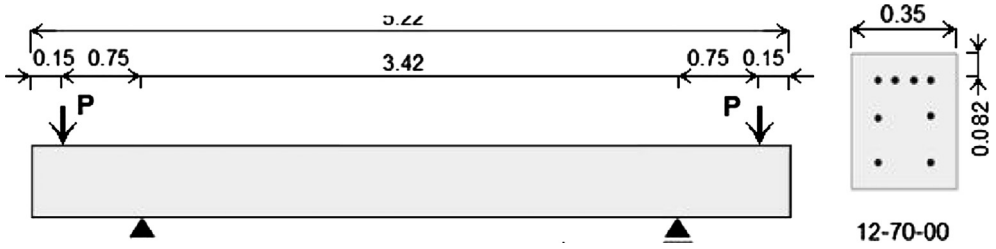

Fig. 19. Geometry of the crack width experiment by Caldentey and et al. [5]

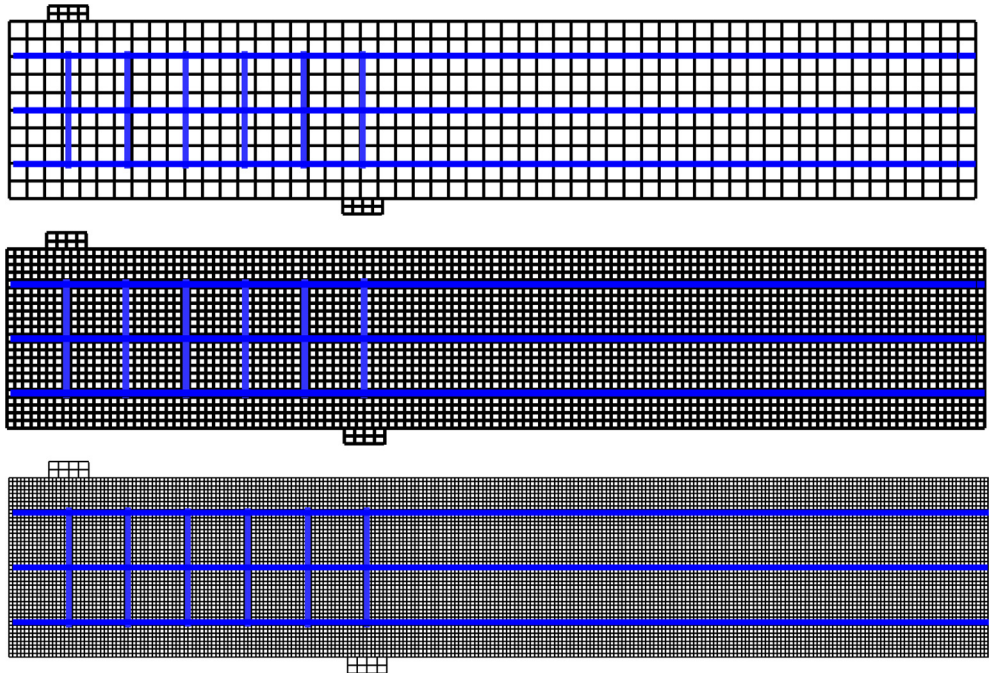

Fig. 20. Finite element meshes for Caldentey crack width experiment, mesh sizes 45, 20 and 10 mm.

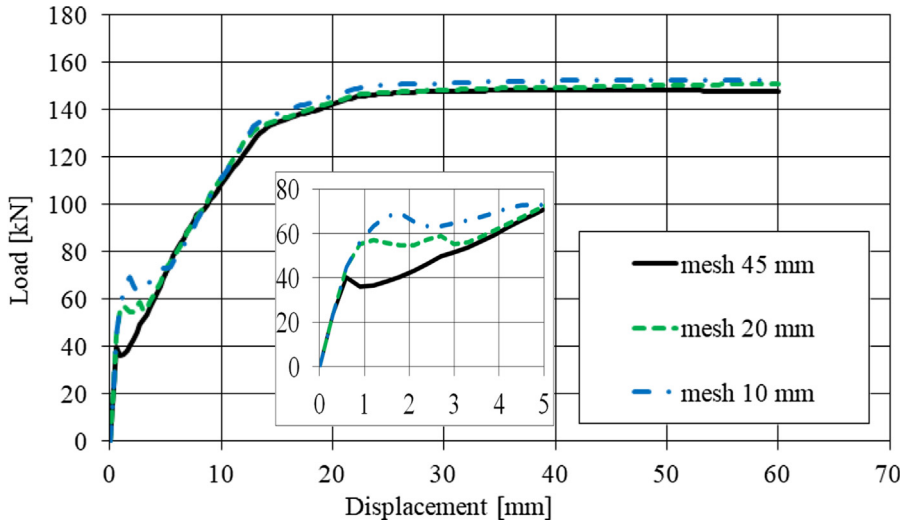

Fig. 21. Load diagram for the crack width example for different mesh sizes without crack spacing limits.

deflections in the range of 1–5 mm. This difference may seem insignificant if one observes the overall load-displacement diagram, but becomes quite significant if we focus only on this initial response after the crack initiation. For instance, for the load of 60kN the analysis with mesh size 10 mm without the spacing limiters provides beams deflection of 1 mm (Fig. 21), while the same analysis with the spacing limiters in Fig. 22 gives the deflection of 4 mm. This is a huge difference that may be very significant for instance if nonlinear analysis is used for service limit state verification. This large difference can be explained by close examination of the crack patterns in these two cases.

This comparison is provided in Fig. 23. It clearly shows the detrimental effect of the initialization of too many parallel cracks that are able to dissipate excessive amount of energy and slow the crack propagation and localization. This effect was already discussed in Section 5, when the crack spacing limiters were introduced. The localization limiter in this case makes the response of each crack slightly more brittle, and it compensates for the incorrect, too fine, crack spacing.

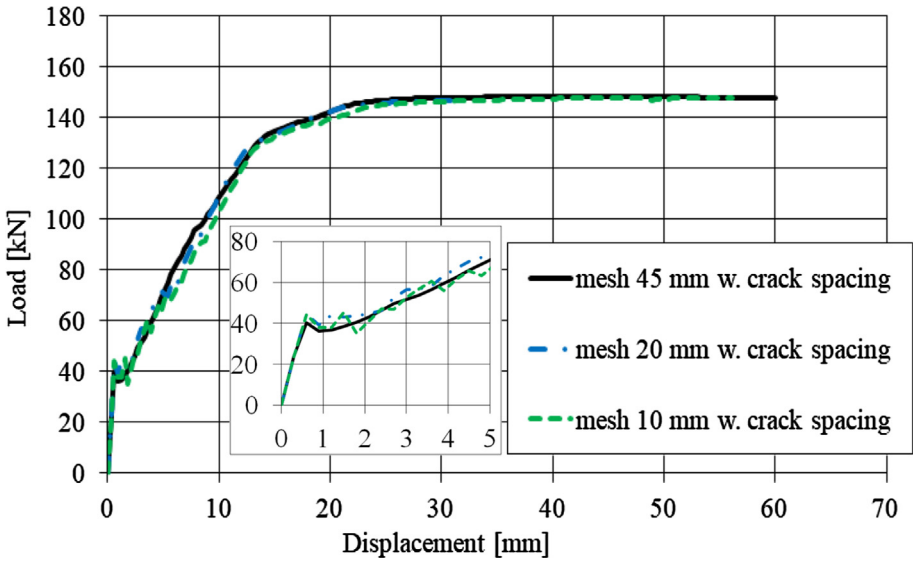

Fig. 22. Load diagram for the crack width example for different mesh sizes with crack spacing limits.

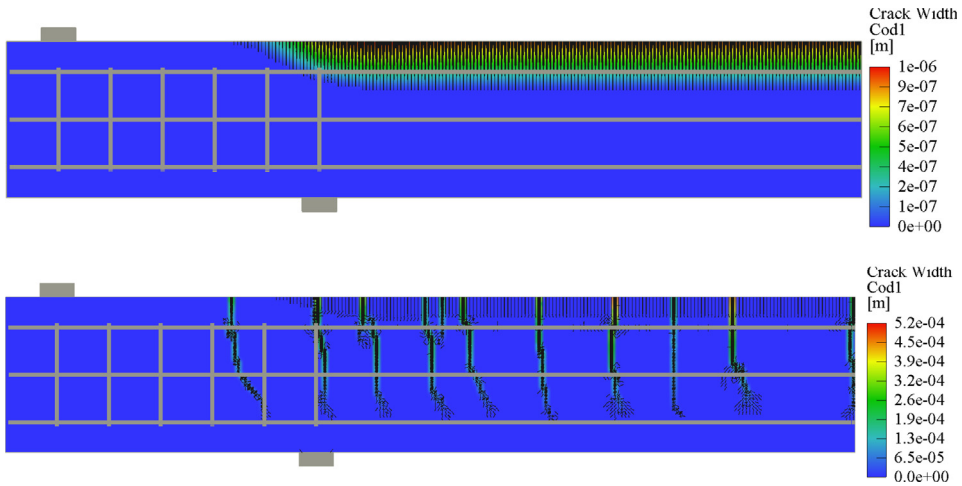

Fig. 23. Comparison of crack patterns at the load 60 kN for the analysis without spacing limiters (top) and results for the case with localization limiters (bottom).

5.3. Cylindrical compression test

The assumption of limiting crush band size $L_c^{\lim}$ was tested on the same cylindrical tests of [26] (Fig. 10) using different mesh sizes 15, 30 and 60 mm. Fig. 24 shows the typical response of the cylindrical test analysis when fine mesh is used. The figure clearly shows that in the case of the compression failure, the damage cannot localize into a single element as is the underlying assumption of the crush band model. This is due to the complex nature of the compression failure, where the dilatancy caused by plastic strains development will always involve surrounding elements into the crushing process. The crush band method should normally make the smaller elements more ductile, which would result in too ductile overall behavior as was the case reported in Fig. 11 (right). The localization limiter limits the ductility of the small elements such that the ductility of the overall response is not increasing excessively if small elements are used. The calculated responses of the cylindrical tests with the localization limiter are reported in Figs. 25–27. It can be seen that the calculated results correctly reproduce the expected increase of brittleness for larger specimens, but the accuracy deteriorates as the element size increases. This is caused by the fact that for element size 60 mm, there are only 2–3 elements across the specimen diameter and in the localization limiter L_c = 150 mm. This model cannot accurately capture the strain and stress localization and distribution over the specimen involving only 2–3 elements. Nevertheless the results still capture properly the size effect and the inaccuracy remains within the limits of concrete material uncertainty and randomness.

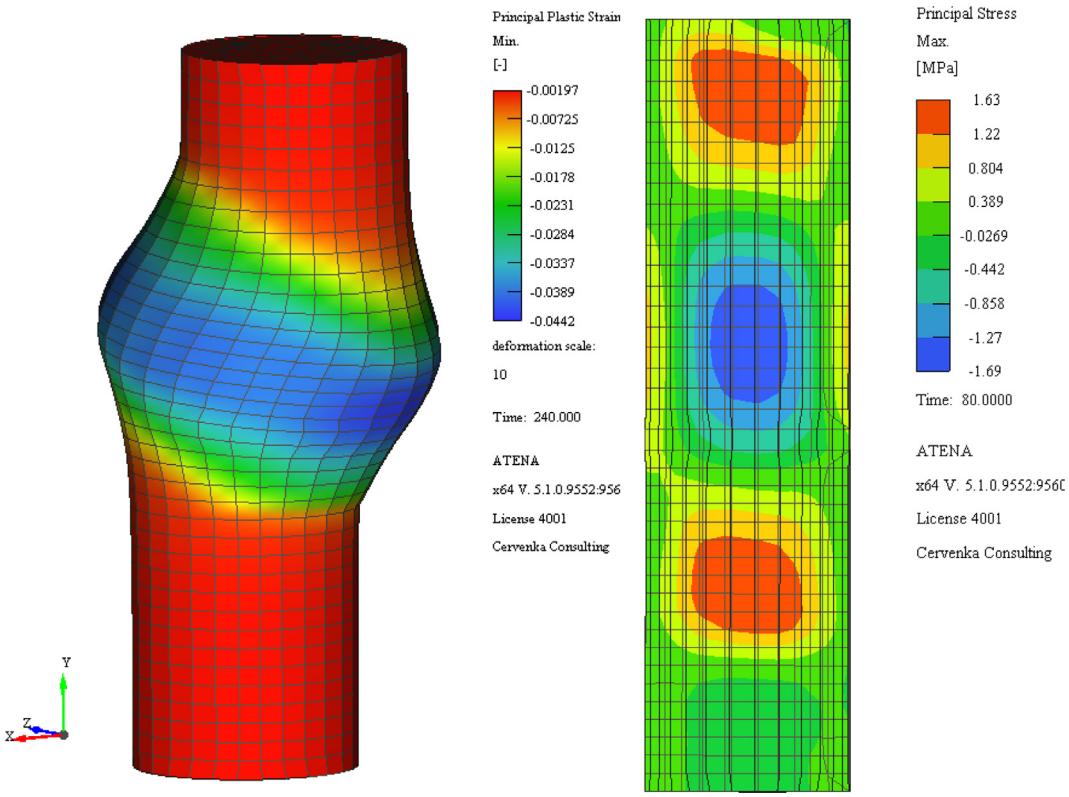

Fig. 24. Failure mode, damage localization and stress confinement in the analysis of cylindrical compression tests [26].

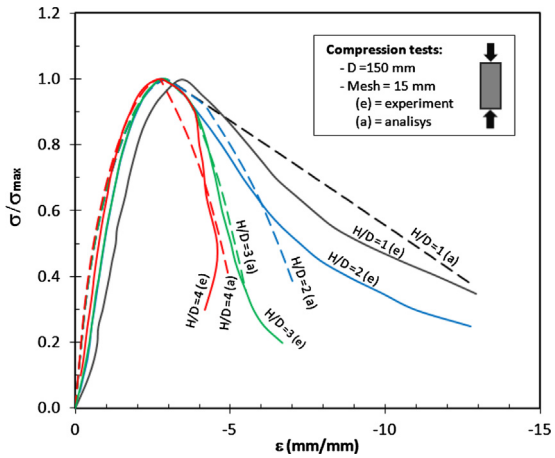

Fig. 25. Response curves for cylindrical specimens for element size 15 mm.

5.4. Rotational capacity of reinforced concrete beams in bending

The proposed method was also verified using the reinforced concrete beams tested by Bosco and Debenardi [4]. Accurate modeling of compressive crushing is important for the prediction of rotational capacity of reinforced concrete beams. For beams with low reinforcement ratio, the strength and the rotational capacity is mainly given by the yielding strength of reinforcement and its critical elongation at rupture.

For beams with high reinforcement ratio, the strength as well the rotational capacity is controlled by the capacity of the compressed section to absorb high compressive strains without significant softening. The experimental results of Bosco and Debenardi [4] were used to evaluate if the proposed model can correctly reproduce the different failure modes observed in the experiments, i.e. mainly the switch between the reinforcement rupture and concrete crushing mode of failure.

The geometry and reinforcement arrangement of the analyzed beams is described in Fig. 28. Two beam dimensions were

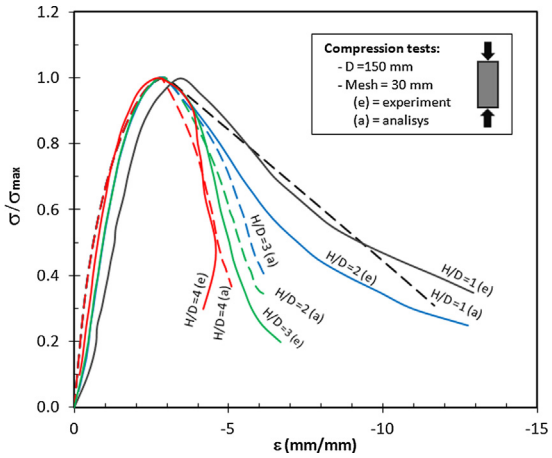

Fig. 26. Response curves for cylindrical specimens for element size 30 mm.

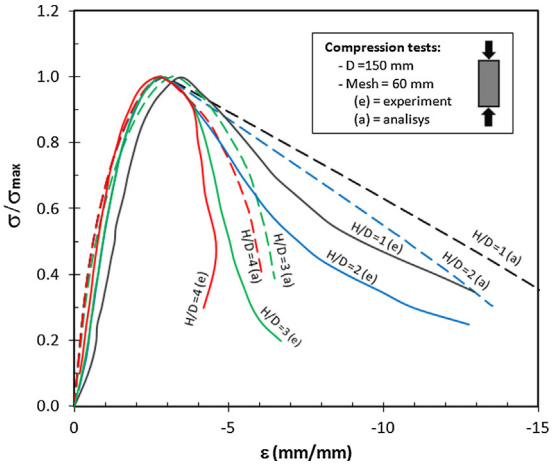

Fig. 27. Response curves for cylindrical specimens for element size 60 mm.

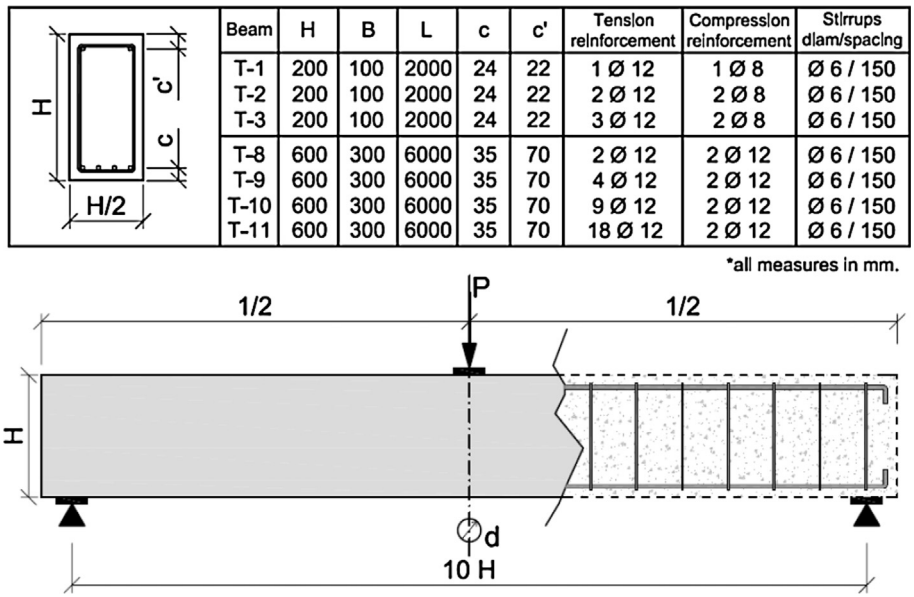

Beam	H	B	L	c	c'	Tension reinforcement	Compression reinforcement	Stirrups diam/spacing
T-1	200	100	2000	24	22	1 Ø 12	1 Ø 8	Ø 6 / 150
T-2	200	100	2000	24	22	2 Ø 12	2 Ø 8	Ø 6 / 150
T-3	200	100	2000	24	22	3 Ø 12	2 Ø 8	Ø 6 / 150
T-8	600	300	6000	35	70	2 Ø 12	2 Ø 12	Ø 6 / 150
T-9	600	300	6000	35	70	4 Ø 12	2 Ø 12	Ø 6 / 150
T-10	600	300	6000	35	70	9 Ø 12	2 Ø 12	Ø 6 / 150
T-11	600	300	6000	35	70	18 Ø 12	2 Ø 12	Ø 6 / 150

*all measures in mm.

Fig. 28. Geometry of the beam specimens [4].

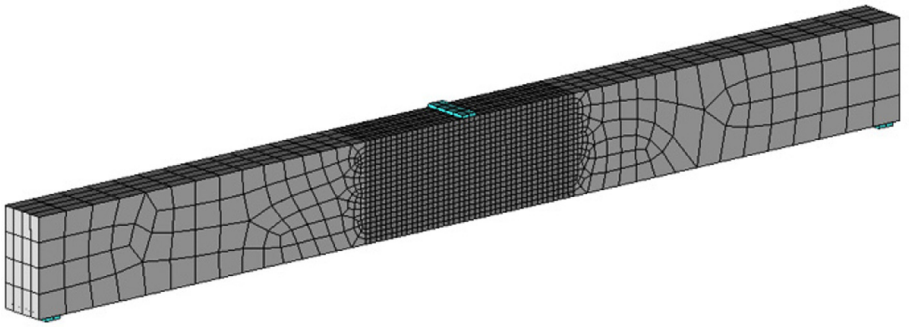

Fig. 29. Typical mesh for the beam specimens with mesh size in the middle section 30 mm.

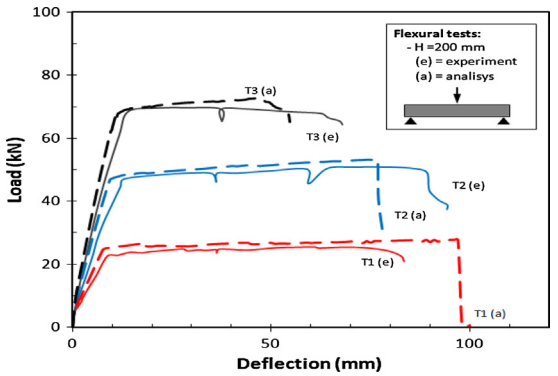

Fig. 30. Response curves for small beams Bosco and Debenardi [4].

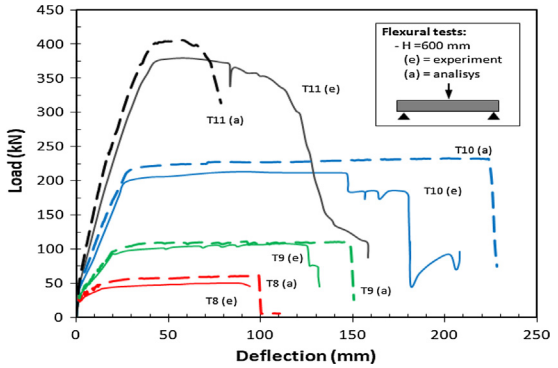

Fig. 31. Response curves for large beams Bosco and Debenardi [4].

considered: small beams with the dimension 100 × 200 × 2000 mm and larger beams with 300 × 600 × 6000 mm. For each beam dimension, several reinforcement ratios are considered, which should demonstrate the switch of the various failure modes.

The typical finite element mesh is shown in Fig. 29. The reinforcement is modeled using the embedded approach and the bond model by Jendele and Cervenka [22]. For the both beam types the element size in the middle zone was 30 mm. The limiting value of $L_{c,\min}$ can be estimated by the minimal beam dimension as discussed in Section 5.

The resulting load-displacement graphs are shown in Figs. 30 and 31 for the small and large beams respectively. The beams with lower reinforcement ratio failed by reinforcement rupture (Fig. 32a). This was the case of beams T1-2, T8-10. The reinforcement yield strength was 565 MPa, and tensile strength was 672 MPa at the critical strain of 7%. The concrete crushing (Fig. 32b) was observed only for the cases with the highest reinforcement ratio, i.e. beams T3 and T11. The graphs for T3 and T11 in Figs. 30 and 31 on the other hand show slightly too brittle response of the numerical model compare to the experimental one. It should be also noted that the post-peak softening was not known for the used concrete type so the same w_d was assumed as in the cylindrical models from the third validation problem.

The problem of compressive softening is still not well understood also from the experimental point of view since the w_d values suggested by the two experimental works by Van Mier [33] and Nakamura & Higai [26] are quite different. Van Mier proposes the

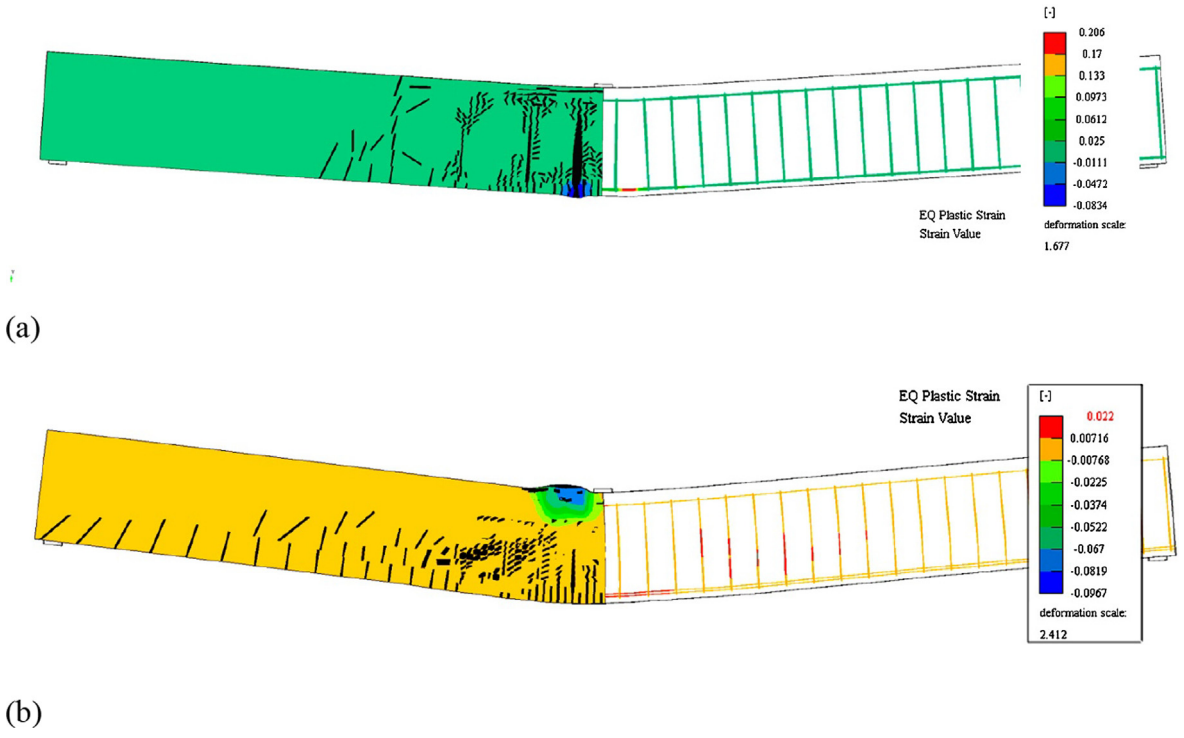

Fig. 32. Failure mode for large beams [4] with low reinforcement ratio with reinforcement rupture (a) and high reinforcing ratio with concrete crushing (b).

value of 0.5 mm, while the experiments of Nakamura & Higai suggests the value of 2.5 mm.

It is therefore highly recommended to always validate the model on suitable experimental results before applying it to practical engineering problems. The validation should be always performed using experiments, which show failure modes that are expected in the real structure. This reduces the model uncertainties and increases the reliability of the numerical simulation.

6. Conclusions

The crack band method is by far the most successful approach in modeling of nonlinear behavior of reinforced concrete structures. The paper discusses the extension of the crack band approach also for compressive softening. The crack band method as well as its dual counterpart the crush band method is used in finite element modeling of reinforced concrete structures to reduce the dependency of results on finite element mesh sizes. Its main objective is to guarantee the proper energy dissipation during the fracturing or crushing process. The paper discusses that this successful approach works very well in most cases, but if too small or too large finite element sizes are used the crack band method does not provide mesh size independent results anymore. This becomes important namely if reinforcement is considered and when applying the method for compressive softening.

Three localization limiters are proposed:

$L_{t,\min}$ – minimal crack spacing limiter in tension related to aggregate size
$L_{t,\max}$ – maximal crack spacing limiter in tension related to reinforcement arrangement
$L_{c,\min}$ – minimal crush band limiter in compression related to the minimal size of the compression zone

Table 1 shows that in case of the strict application of these limiters, the finite element size in reinforced concrete analysis should be limited to 150 mm in typical situations, which would be an extremely restrictive condition.

The paper proposes a simple approach how these limiters could be used in practical finite element analyses with varying mesh sizes yet preserving sufficient accuracy of the finite element results.

This approach was validated using four examples with known experimental results. Reinforced concrete shear panel was used to verify the model performance for large as well as small mesh sizes. Four point bend beams were used to demonstrate the model behavior in serviceability limits states for deflection as well as crack width estimation. The crush band model was validated on uniaxial compression tests and by comparing results for the rotational capacity of reinforced concrete beams in flexure. The model is able to capture the main features of reinforced concrete behavior.

Proper investigation and assessment of model uncertainties or input parameter sensitivity studies should be always performed when applying nonlinear analysis to practical engineering problems.

The presented results are based on research performed within the project 16-04132S "Epistemic uncertainties in crack models in reinforced concrete structures" from Czech grant agency.

References

[1] Bažant ZP. Instability, ductility and size effect in strain softening concrete. J Eng Mech ASCE 1976;102(2):331–44.
[2] Bažant ZP, Oh BH. Crack band theory for fracture of concrete. Mater Struct RILEM 1983;16(3):155–77.
[3] Bažant ZP, Pijaudier-Cabot G. Nonlocal continuum damage, localization instability and convergence. J Appl Mech ASME 1987;55(2):287–93.
[4] Bosco C, Debenardi PG. Influence of some basic parameters on the plastic rotation of reinforced elements. Ductility requirements for structural Concrete – Reinforcement Comite Eruo-international du Breton CEB bulletin 1993;218:25–44.
[5] Caldentey PA, et al. Cracking of RC members revisited: influence of cover, $\phi/\rho_{s,\ ef}$ and stirrup spacing – an experimental and theoretical study. Struct Concr 2013;14(1):69–78.
[6] Collins MP, Bentz EC, Quach PT, Proestos GT. Challenge of predicting the shear strength of very thick slabs. Concr Int 2015;37(11):29–37.
[7] Červenka J, Červenka V, Laserna S. On finite element modelling of compressive failure in brittle materials. In: Bicanic et al., editors, Computational Modeling of Concrete Structures Euro-C 2014, St. Anton, Austria, Tazlor & Francis Group, London, ISBN 978-1-138-00145-9; 2014. p. 273–81.
[8] Červenka J, Červenka V, Eligehausen R. Fracture-plastic material model for concrete, application to analysis of powder actuated anchors. Proc FRAMCOS 1998;3(1998):1107–16.
[9] Červenka J, Papanikolaou V. Three dimensional combined fracture-plastic material model for concrete. Int J Plast 2008;24:2192–220.
[10] Červenka V, Gerstle K. Inelastic analysis of reinforced concrete panels. Part I: Theory. Publication I.A.B.S.E. 1971;31(11):32–45.
[11] Červenka V, Gerstle K. Inelastic analysis of reinforced concrete panels. Part II: Experimental Verificatin and Application. Publication I.A.B.S.E. 1972;32(11):25–39.
[12] Červenka V, Červenka J, Jendele L. ATENA Program Documentation, Part 1: Theory, 2018, Cervenka Consulting s.r.o.; 2018, www.cervenka.cz.
[13] Červenka V, Marková J, Mlčoch J, Caldentey AP, Sajdlová T, Sýkora M. Uncertainties of Crack Width Models, fib Symposium 2017, Maastricht; 2017.
[14] Červenka V, Pukl R, Ozbold J, Eligehausen R. Mesh sensitivity effects in smeared finite element analysis of concrete fracture. In: Proc. Fracture Mechanics of Concrete Structure II, Vol. II, ISBN 3-905088-12-6; 1995. p. 1387–96.
[15] Červenka V. Reliability-based non-linear analysis according to Model Code 2010. J FIB Struct Concr 01/2013 2010;01(2013):19–28.
[16] Červenka V, Marková J, Mlčoch J, Caldentey AP, Sajdlová T, Sýkora M. Uncertainties of crack width models, fib symposium 2017, Maastricht; 2017.
[17] de Borst R. Non-linear analysis of frictional materials. PhD Thesis. Delft University of Technology, The Netherlands; 1986.
[18] de Borst R, Rots JG. Occurence of spurious mechanisms in computations of strain-softening solids. Eng Comput 1989;6:272–80.
[19] de Borst R, Mühlhaus HB. Gradient dependant plasticity: formulation and algorithmic aspects. Int J Numer Meth Eng 1992;35(3):521–39.
[20] de Borst R, Benallal A, Heeres OM. A gradient-enhanced damage approach to fracture. J de Physique IV 1996;C6:491–502.
[21] Etse G. Theoretische und numerische untersuchung zum diffusen und lokalisierten versagen in beton. PhD Thesis. University of Karlsruhe; 1992.
[22] Jendele L, Cervenka J. Modelling bar reinforcement with finite bond. Comput Struct 2006;84:1780–91.
[23] Lee J, Fenves GL. Plastic-damage model for cyclic loading of concrete structures. J Eng Mech ASCE 1998;124(8):892–900.
[24] Lin CS, Scordelis A. Nonlinear analysis of RC shells of general form, ASCE. J Struct Eng 1975;101(3):152–63.
[25] Model Code 2010. First complete draft. Volume 1 – fib bulletin 55. Volume 2 – fib bulletin 56. ISSN 1562–3610. ISBN 978-2-88394-095-6. International Federation for Structural Concrete (fib), Lausanne, Switzerland; 2010.
[26] Nakamura H, Higai T. Compressive fracture energy and fracture zone length of concrete. Modeling of Inelastic Behavior of RC Structures under Seismic Loads: ASCE; 2001. p. 471–87.
[27] Ngo D, Scordelis AC. Finite element analysis of reinforced concrete beams. J Am Concr Inst 1967;64:152–63.
[28] Pramono E, Willam KJ. Fracture energy-based plasticity formulation of plain concrete. J Eng Mech ASCE 1989;115(6):1183–204.
[29] Rashid YR. Analysis of prestressed concrete pressure vessels. Nucl Eng Des 1968;7(4):334–44.
[30] Rots JG, Blaauwendraad J. Crack models for concrete: discrete or smeared? Fixed, multi-directional or rotating? Heron 1989;34(1).
[31] Slobbe AT, Hendriks MAN, Rots JG. Systematic assessment of directional mesh bias with periodic boundary conditions: applied to the crack band model. Eng Fract Mech 2013;109:186–208.
[32] Suidan M, Schnobrich WC. Finite element analysis of reinforced concrete, ASCE. J Struct Div 1973;99(ST10):2108–21.
[33] Van Mier JGM. Multiaxial strain softening of concrete. Part I: fracture. Materials and structures. RILEM 1986;19(111):179–90.
[34] Menetrey P, Willam KJ. Triaxial failure criterion for concrete and its generalization. ACI Struct J 1995;92:311–8.